SANDIA REPORT
SAND2008-1900
Unlimited Release
Printed March 2008

Screening Analysis of Solar Thermochemical Hydrogen Concepts

Gregory J. Kolb and Richard B. Diver

Prepared by
Sandia National Laboratories
Albuquerque, New Mexico 87185 and Livermore, California 94550

Sandia is a multiprogram laboratory operated by Sandia Corporation,
a Lockheed Martin Company, for the United States Department of Energy's
National Nuclear Security Administration under Contract DE-AC04-94AL85000.

Issued by Sandia National Laboratories, operated for the United States Department of Energy by Sandia Corporation.

Available to DOE and DOE contractors from
U.S. Department of Energy
Office of Scientific and Technical Information
P.O. Box 62
Oak Ridge, TN 37831

Telephone: (865) 576-8401
Facsimile: (865) 576-5728
E-Mail: reports@adonis.osti.gov
Online ordering: http://www.osti.gov/bridge

Available to the public from
U.S. Department of Commerce
National Technical Information Service
5285 Port Royal Rd.
Springfield, VA 22161

Telephone: (800) 553-6847
Facsimile: (703) 605-6900
E-Mail: orders@ntis.fedworld.gov
Online order: http://www.ntis.gov/help/ordermethods.asp?loc=7-4-0#online

SAND2008-1900
Unlimited Release
Printed March 2008

Screening Analysis of Solar Thermochemical Hydrogen Concepts

Gregory J. Kolb
Solar Systems Department

Richard B. Diver
Solar Technologies Department

Sandia National Laboratories
P.O. Box 5800
Albuquerque, New Mexico 87185-1127

Abstract

A screening analysis was performed to identify concentrating solar power (CSP) concepts that produce hydrogen with the highest efficiency. Several CSP concepts were identified that have the potential to be much more efficient than today's low-temperature electrolysis technology. They combine a central receiver or dish with either a thermochemical cycle or high-temperature electrolyzer that operate at temperatures >600 ^{o}C. The solar-to-hydrogen efficiencies of the best central receiver concepts exceed 20%, significantly better than the 14% value predicted for low-temperature electrolysis.

TABLE OF CONTENTS

INTRODUCTION 7

TOWER CONCEPTS 7

DISH CONCEPTS 11

SCREENING BASED ON SOLAR-TO-HYDROGEN EFFICIENCY 12
- Molten-Salt Plant Calculations 13
- Solid-Particle-Receiver Plant Calculations 15
- CPC/SiC Reactor Plant Calculations 18
- Dish Plant Calculations 20

CONCLUSIONS 21

REFERENCES 22

LIST OF FIGURES

Figure 1. Solar tower, dish, and trough power plants 8
Figure 2. Tower receiver concepts 10
Figure 3. Solar collection efficiency. 13
Figure 4. DELSOL Solar Tower Optimization Tool 17
Figure 5. Compound parabolic concentrators. 19

LIST OF TABLES

Table 1. Solar Tower Screening Results 9
Table 2. Solar Dish Screening Results 10
Table 3. Optical Efficiencies for Solar Towers (Annual) 14
Table 4. Optical Efficiencies for Solar Dishes (Annual) 15
Table 5. Receiver Efficiencies for Solar Towers (Annual) 16
Table 6. Receiver Efficiencies for Solar Dishes (Annual) 17

INTRODUCTION

Today's concentrating solar power plants (Figure 1) can be used to make hydrogen on a large scale. Low-temperature electrolyzers could be used to convert solar electricity to hydrogen but this process is relatively inefficient. For example, the power plant converts solar heat to electricity at a net (i.e., after parasitic loss) efficiency of 33 to 38%. This electricity would then be converted to hydrogen by a conventional electrolyzer with an efficiency of ~80% (on a High Heating Value (HHV) basis), for a net "heat-to-hydrogen" conversion efficiency of ~26 to 30%.

Overall conversion efficiency can be increased if solar heat is directly converted to hydrogen via a thermochemical process. More than 200 thermochemical cycles have been identified during the last 25 years [1, 2] and several of these are predicted to convert heat to hydrogen at efficiencies > 40% for cycles that operate in the range of 600 to 2000 ^{o}C. During our initial screening of thermochemical cycles for solar application, we limited our search to those with predicted HHV efficiencies that exceeded 40% because they have the best chance of significantly beating the economics of conventional solar-powered electrolysis. These cycles, operating temperatures, and efficiencies are listed in columns 2, 3, and 6 of Tables 1 and 2. Reference 2 gives a complete description of each cycle, as identified by a process identification number (PID, listed in column 1).

Since >600 ^{o}C is needed to achieve 40% efficiency and since solar troughs operate well below this temperature, trough technology was eliminated from further consideration. Towers and dishes, however, concentrate light to much higher levels than troughs and are thus capable of achieving temperatures much greater than 600 ^{o}C. The next task was to identify tower and dish receiver concepts that match the operating temperatures of each thermochemical cycle that exceeded 40% efficiency.

TOWER CONCEPTS

Current molten-salt technology (Solar Two, Figure 1) can be used to supply 600 ^{o}C heat to the Copper Chloride cycle (PID 191, Table 1). Up to 13 hours of molten salt can be economically stored in tanks to power the thermochemical plant "around the clock." Simulations suggest that up to a 75% annual capacity factor can be achieved for a plant located in the Mojave Desert. A high capacity factor implies fewer startups of the thermochemical plant, which results in an improved annual efficiency of converting heat to hydrogen.

To achieve the higher temperatures listed in Table 1 will require the development of new receiver concepts. Starting with a review of high-temperature solar power tower concepts introduced in the 1970s and 1980s for thermochemical and Brayton applications [3, 4], we used our many years of power tower development experience to identify candidate tower-receiver technologies that are capable of >850 ^{o}C. The candidate receiver technologies are depicted in Figure 2. Tubular, heat pipe, and volumetric concepts appear to be feasible up to ~1000 ^{o}C. Solid particle receivers may be feasible to ~1500 ^{o}C, but are better suited to <1200 ^{o}C. To achieve very high temperatures (>1500 ^{o}C) with a good receiver efficiency, high solar concentrations (>5000) are necessary; this necessitates the incorporation a compound parabolic concentrator (CPC) at the entrance of the receiver [5].

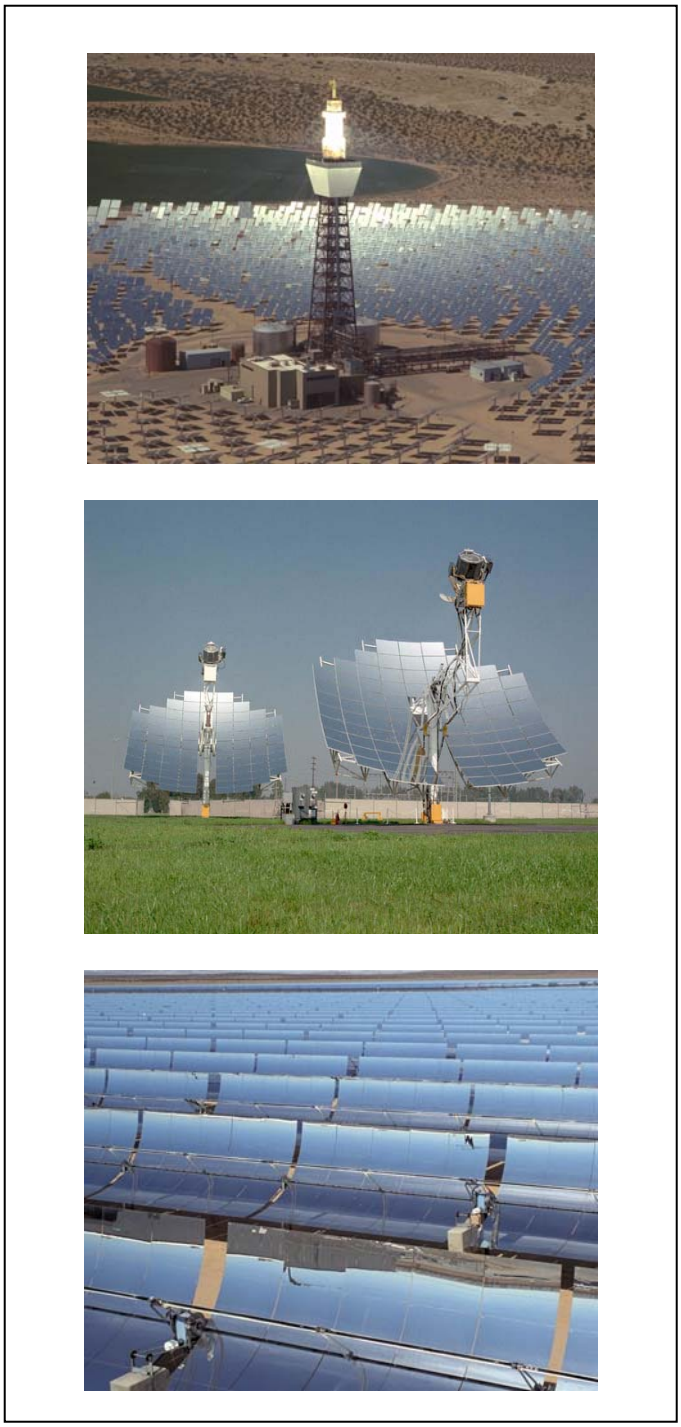

Figure 1. Solar tower, dish, and trough power plants

Table 1. Solar Tower Screening Results

PID	Cycle Name	Chemical Cycle Temp (^{o}C)	Solar Plant	Solar Receiver & Size (MWt)	T/C η (HHV)	Optical η from Table 3	Rcvr η from Table 5	Annual S-to-H η
0	Conventional Electrolysis **BASELINE**	NA	Current Power Tower (PT)	Molten Salt 700	30%	57%	83%	14%
106	Hi-T Steam *Electrolysis*	850	Future PT	Solid Particle 700	45%	57%	76.2%	20%
191	Copper/Hybrid *Chloride*	600	Current PT	Molten Salt 700	49%	57%	83%	23%
67	Hybrid *Sulfur*	850	Future PT	Solid Particle 700	51%	57%	76%	22%
1	*Sulfur* Iodine	850	Future PT	Solid Particle 700	45%	57%	76%	19%
5	Cadmium/Hybrid *Metal Oxide*	1450	Future PT	Solid Particle 700	50% to 70%*	50%	67%	20%
182	Cadmium Carbonate *Metal Oxide*	1450	Future PT	Solid Particle 700	50% to 70%*	50%	67%	20%
6	Zinc *Metal Oxide*	1800	Future PT	CPC Si-G Reactor 46	45%	51%	72%	16.5%
110	Manganese *Metal Oxide*	1550	Future PT	CPC Si-G Reactor 46	50%	55%	78%	21%
131	Manganese *Sulfate* **	1500	Future PT	Solid Particle 700	42%	50%	67%	14%
147	Cadmium *Sulfate* **	1150	Future PT	Solid Particle 700	55%	54%	73%	22%
149	Barium Molybdenum *Sulfate* **	1400	Future PT	Solid Particle 700	47%	50%	67%	16%

* 60% was used in the calculation.

** After completing this screening analysis, sulfate cycles were eliminated from further consideration because experimental evidence indicated that the hydrolysis reaction did not work as originally suggested by analytical studies [2].

Table 2. Solar Dish Screening Results

PID	Cycle Name	Chemical Cycle Temp (°C)	Solar Plant	Solar Receiver & Size (kWt)	T/C η	Optical η from Table 4	Rcvr H from Table 6	Annual S-to-H η
00	Conventional Electrolysis **BASELINE**	NA	Current Dish	Stirling	26%	85%	86%	19%
106	Hi-T Steam *Electrolysis*	900	Future Dish	Stirling and Steam	35%	85%	84%	25%
2	Nickel-Iron Manganese *Ferrite*	1800	Future Dish	Rotating Disk	52%	77%	62%	25%
7	Iron Oxide *Ferrite*	2100	Future Dish	Rotating Disk	50%	74%	62%	23%
194	Zinc *Ferrite*	1800	Future Dish	Rotating Disk	52%	77%	62%	25%

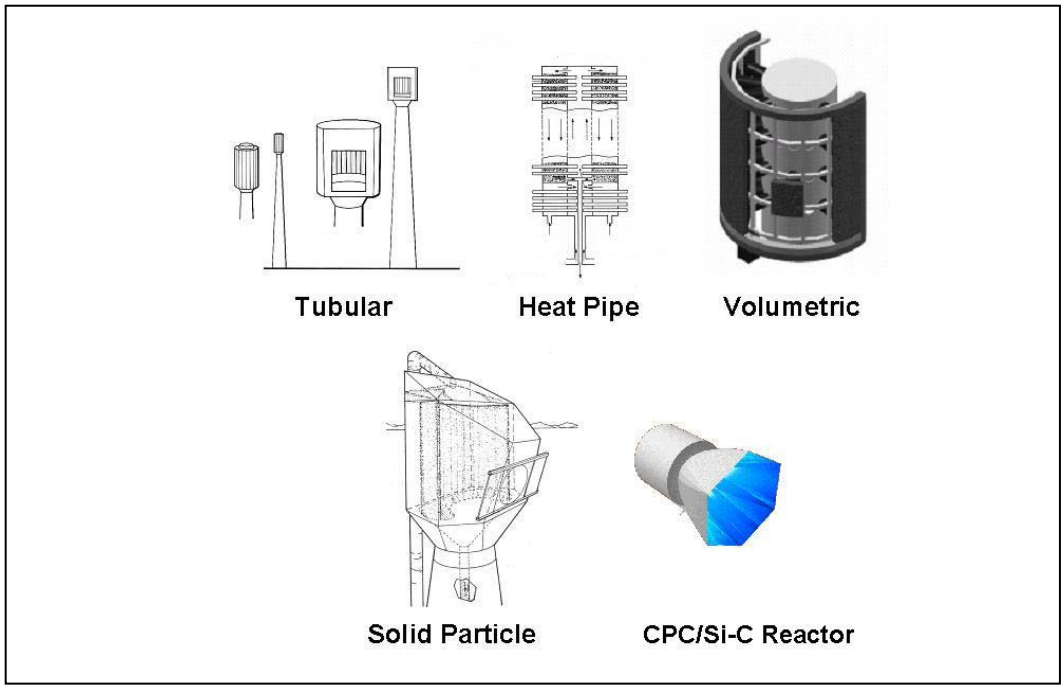

Figure 2. Tower receiver concepts

Upon further examination we eliminated receiver concepts with serious issues related to environmental, safety, and health (ES&H) concerns or material-lifetime. For example, tubular and heat-pipe receivers that contained liquid sodium, cadmium, or sulfuric acid were dropped because leaks would result in a dangerous situation. We also eliminated receiver concepts that would likely have poor heat-collection efficiency. For example, the volumetric receiver was eliminated because it is difficult to recuperate heat at high temperatures (~60% for the volumetric vs. >90% for other receiver designs). The remainder of the analysis thus focused on the solid particle and CPC receivers.

The solid-particle receiver was investigated in the mid-1980s for solar Brayton and thermochemical applications [6]. Blackened alumina particles, the size of common beach sand, directly absorb the solar energy as it falls within an open cavity receiver. Because the "sand" has a high heat capacity and is inexpensive, it is cost-effective to store the heated sand within a silo for later use. Like molten salt technology, 13 hours of thermal storage can be economically integrated into the design. Heat is transferred from the sand to the thermochemical plant via a tube and shell heat exchanger [7] or by heat exchanger technology now used in fluidized-bed coal plants. By the time the work ceased in 1987 (as a result of reduced funding) the researchers had characterized solid-particle materials, developed a computational model to simulate particle dynamics and receiver thermal performance, and performed a number of small-scale particle drop tests. Analysis predicted relatively high receiver efficiency (~80%) but no on-sun receiver tests were performed to verify this. Referring to Table 1, the solid particle receiver is recommended for all thermochemical cycles in the range of 850 to 1500 ^{o}C. It is also recommended for high-temperature steam electrolysis (PID 106).

The CPC receiver concentrates sunlight several thousand times to heat several reactor tubes enclosed in a cavity structure. A metal oxide aerosol, the size of talcum powder, flows within the tubes and is quickly heated from 1500 to 1800 ^{o}C, depending on the process. This heating reduces the metal oxide into metal and oxygen. Metal powder can be stored for an indefinite period of time for later reaction with water to produce hydrogen. This inherent chemical energy storage is a desirable feature. In the current receiver concept being developed by University of Colorado (UC) and NREL [2], approximately 30 silicon-carbide tubes (each with a diameter of 0.6 m) are heated via three CPC concentrators. This receiver concept is based on commercially available graphite-tube reactors that operate at over 1800 ^{o}C to produce tungsten carbide. UC and NREL are currently developing analytical and experimental tools to estimate receiver efficiency. Receiver efficiencies presented in this paper are first-order estimates and need to be updated in the future. Referring to Table 1, the CPC receiver is recommended for thermochemical cycles above 1500 ^{o}C; all of these are metal oxide cycles.

DISH CONCEPTS

Current dish concentrators (Stirling Energy Systems, Figure 1) provide high-temperature heat at about 800 ^{o}C to high-performance Stirling engine/induction generator power conversion units (PCUs) located near the focal point. State-of-the-art solar concentrators typically operate with an average aperture concentration ratio in the range of 2000 to 3000 suns with high intercept factors (99%). They are capable of 4000 suns with an intercept of 95%. However, because of the

relatively small scale and distributed nature of parabolic dishes and especially the need to accommodate variable orientations, the number of thermochemical cycles suitable for parabolic dishes is limited. Any thermochemical cycle for a parabolic dish must, therefore, be simple and the receiver/reactor must accommodate variable orientations relative to gravity, as well as the requirements of the thermochemical cycle.

Only the Ferrite cycles, represented by PIDs 2, 7, and 194 and implemented in the Sandia-invented rotation disk reactor, meet the requirements of parabolic dishes. In the rotating disk reactor, the solid iron/mixed metal oxide is supported on a solid matrix and is, therefore, capable of operating in a variable gravity orientation environment. The rotating disk reactor also accommodates separation of the product hydrogen and oxygen and sensible heat recuperation needed for high efficiency.

The Ferrite cycles in Table 2 are representative of a potentially large number of viable thermochemical cycles based on iron oxide mixed with various amounts of nickel, manganese, magnesium, cobalt, zinc or combination oxides. They are representative of the efficiency potential and temperatures required as calculated with realistic heat transfer and other assumptions using thermodynamic data in HSC Chemistry for Windows [8]. Note that the pure Iron Oxide cycle (PID 7) requires a higher temperature than the mixed-metal Ferrite cycles.

SCREENING BASED ON SOLAR-TO-HYDROGEN EFFICIENCY

The next step in the screening process was to estimate the solar-to-hydrogen efficiency for each proposed solar-thermochemical plant. This efficiency is the product of solar-collection and thermochemical-cycle efficiencies. Variations in weather, sun position, and sun intensity cause the efficiency of a solar plant to change throughout the day and throughout the year. Thus, it is necessary to estimate solar-collection efficiency on an annual basis. This effect is illustrated in Figure 3. For the thermochemical cycle efficiency we used a design point rather than an annual efficiency. We believe this is a reasonable assumption at this point. For the power tower cycles that utilize thermal storage, we expect that the storage will buffer solar transients and allow the thermochemical cycle to operate close to design point during most of the year. The remaining metal oxide cycles are relatively simple and reactors and other internal heat transfer process should not degrade with turn down. These assumptions will of course need to be investigated in future studies.

For each tower case we used the DELSOL [9] computer code to estimate the annual solar-collection efficiency. This is done by performing hourly simulations of the heliostat-field optics and the receiver thermal performance for several representative days throughout the year. Annual efficiency is subdivided into optical and receiver efficiencies, as indicated in Tables 1 and 2. To gain a detailed understanding of the differences between the tower systems it is necessary to further subdivide the optical and receiver efficiencies, as shown in Tables 3 through 6.

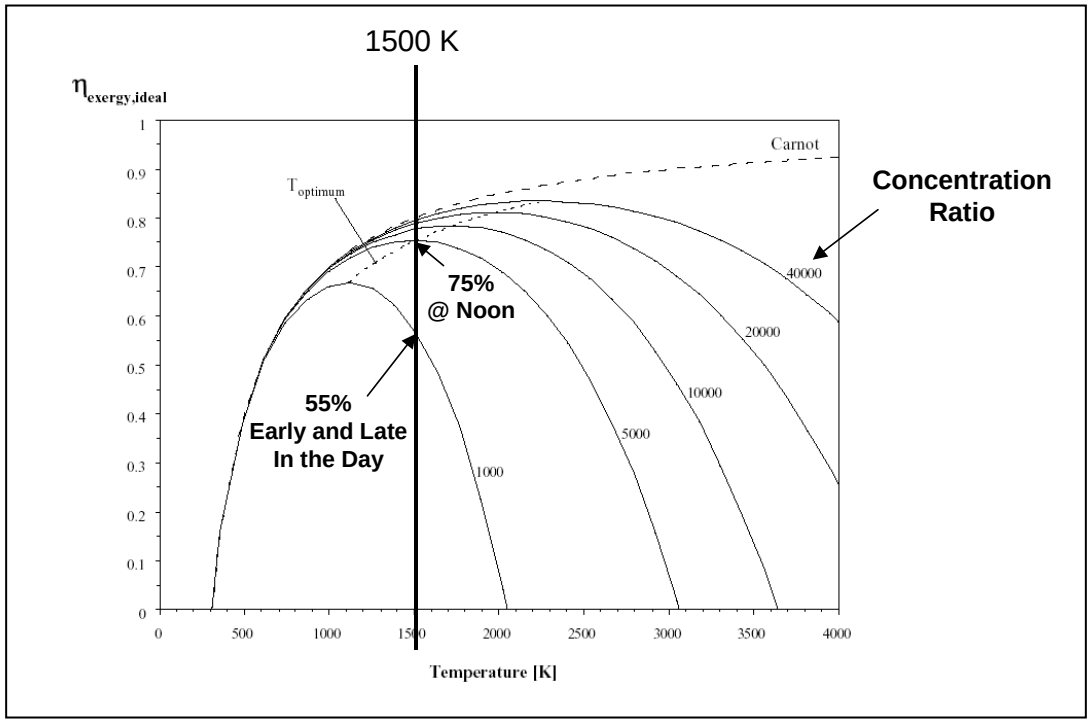

Figure 3. Solar collection efficiency.
The efficiency of a solar receiver varies throughout the day because solar input is changing and thermal losses are constant. The highest efficiency occurs at noon when solar input is highest [5].

The annual efficiency calculated by DELSOL is based on a first-order design that was determined by the code to yield the lowest levelized cost of collected solar energy. DELSOL does this by computing the cost for all possible combinations of tower height, receiver aperture dimensions, and heliostat field layout. The user supplies the cost data (for tower, receiver, and heliostats), the heliostat design, and the receiver thermal losses as a function of aperture area, as well as the receiver power level. The DELSOL algorithm is depicted in Figure 4.

Molten-Salt Plant Calculations

The optimal molten-salt plant was very similar to the year 2008 case study investigated by Sargent & Lundy for the National Academy of Science [10]. This calculation was based on the following DELSOL input:

- Heliostats – 98 m^2; 1.3 mrad slope/tracking error; 94% reflectance; 95% cleanliness; canted/focused to slant range; cost is \$120/m^2 ; heliostats surround the tower.
- Receiver – Reflectivity of receiver surface is 7%; receiver absorbs 700 MWt @ noon; 600 ^oC outlet temperature equates to thermal losses of 31 kW/m^2; default cost algorithms for receiver and tower.

The optimal plant is predicted to use 1.31E6 m^2 of heliostats, a 210-m tower, and a cylindrical receiver with an absorber area of 1000 m^2. Interfacing this plant with the Copper Chloride cycle (PID 191) yields an annual solar-to-hydrogen efficiency of 23%.

Table 3. Optical Efficiencies for Solar Towers (Annual)

PID	Cycle Name	Helio Size (m^2) & Layout	Cosine η	Shade & Block η	Atmos. Atten. η	Aper. Intercept η	CPC η	Opt. η
0	Lo-T Electrolysis **BASELINE**	98 & Surround	76%	97%	91%	96%	NA	57%
106	Hi-T Steam *Electrolysis*	98 & North	85%	96%	88%	90%	NA	57%
191	Copper/Hybrid *Chloride*	98 & Surround	76%	97%	91%	96%	NA	57%
67	Hybrid *Sulfur*	98 & North	85%	96%	88%	90%	NA	57%
1	*Sulfur* Iodine	98 & North	85%	96%	88%	90%	NA	57%
5	Cadmium/Hybrid *Metal Oxide*	98 & North	85%	96%	87%	81%	NA	50%
182	Cadmium Carbonate *Metal Oxide*	98 & North	85%	96%	87%	81%	NA	50%
6	Zinc *Metal Oxide*	98 & North	87%	96%	93%	84%	89%	51%
110	Manganese *Metal Oxide*	98 & North	87%	96%	94%	90%	89%	55%
131	Manganese Sulfate	98 & North	85%	96%	87%	81%	NA	50%
147	Cadmium *Sulfate*	98 & North	85%	96%	88%	86%	NA	54%
149	Barium Molybdenum *Sulfate*	98 & North	85%	96%	87%	81%	NA	50%

Note: Optical efficiency includes four common factors: mirror reflectance (94%), mirror cleanliness (95%), high-wind outage (99%), and field availability (99%).

Table 4. Optical Efficiencies for Solar Dishes (Annual)

PID	Cycle Name	Cosine η	Shade & Block η	Atmos. Atten. η	Aper. Intercept η	CPC η	Window η	Opt. η
00	Lo-T *Electrolysis* **BASELINE**	100%	98%	100%	99%	NA	NA	85%
106	Hi-T Steam *Electrolysis*	100%	98%	100%	99%	NA	NA	85%
2	Nickel-Iron Manganese *Ferrite*	100%	98%	100%	95%	NA	95%	77%
7	Iron Oxide *Ferrite*	100%	98%	100%	95%	96%	95%	74%
194	Zinc *Ferrite*	100%	98%	100%	95%	NA	95%	77%
Note: Optical efficiency includes four common factors: mirror reflectance (94%), mirror cleanliness (95%), high-wind outage (99%), and field availability (99%).								

Solid-Particle-Receiver Plant Calculations

This calculation was based on the following DELSOL input:

- Heliostats – 98 m^2; 1.3 mrad slope/tracking error; 94% reflectance; 95% cleanliness; canted/focused to slant range; cost is \$120/m^2; heliostats are north of the tower.
- Receiver – Receiver absorbs 700 MWt @ noon; 900 ^oC to 1500 ^oC outlet temperature equates to thermal losses of 290 to 680 kW/m^2; default cost algorithms for receiver and tower.

The solid-particle plant calculations were based on the same input assumptions as the molten-salt case, except that receiver thermal losses were increased due to the much higher operating temperatures. The optimal low-temperature plant (e.g., interfaced with PID 67) is predicted to use 1.34E6 m^2 of heliostats, a 360-m tower, and a cavity receiver with an aperture area of 400 m^2 and a downward tilt of 30^o. The optimal high-temperature plant (e.g., interfaced with PID 131) is predicted to use 1.65E6 m^2 of heliostats, a 420-m tower, and a cavity receiver with an aperture area of 300 m^2. Comparing these results with the molten-salt plant yields the following insights:

- A cylindrical receiver is preferred for the molten-salt plant and a cavity-type receiver is preferred for the solid-particle plant. The cavity is required for two reasons: (1) the particles must be protected from the wind to prevent particle loss, and (2) higher thermal losses caused by the higher operating temperature are compensated by a smaller heat-transfer area (i.e., 300 to 400 m^2 for cavity vs. 1000 m^2 for cylindrical). The optimum heat-transfer area defined by DELSOL is a function of receiver flux limits and a trade-off between interception and heat-loss efficiencies. Since the flux limit for the particle receiver is higher and the heat losses are also higher, DELSOL identified a much smaller area as optimum for the particle receiver.

Table 5. Receiver Efficiencies for Solar Towers (Annual)

PID	Cycle Name	Avg Noon Aperture Flux kW/m^2	Aperture Thermal Losses kW/m^2	Absorb η	Radiation η	Convect η	Trans-ient η	Receiver Thermal η
0	Lo-T Electrolysis **BASELINE**	500	31	93%	96.7%	98.9%	93%	83%
106	Hi-T Steam *Electrolysis*	2000	290	100%	90%	91%	93%	76.2%
191	Copper/Hybrid *Chloride*	500	31	93%	96.7%	98.9%	93%	83%
67	Hybrid *Sulfur*	2000	290	100%	90%	91%	93%	76%
1	*Sulfur* Iodine	2000	290	100%	90%	91%	93%	76%
5	Cadmium/Hybrid *Metal Oxide*	3000	680	100%	80%	90%	93%	67%
182	Cadmium Carbonate *Metal Oxide*	3000	680	100%	80%	90%	93%	67%
6	Zinc *Metal Oxide*	1030*	1010**	100%	77%	NA	93%	72%
110	Manganese *Metal Oxide*	850*	620**	100%	83.5%	NA	93%	78%
131	Manganese *Sulfate*	3000	680	100%	80%	90%	93%	67%
147	Cadmium *Sulfate*	2400	420	100%	87%	90%	93%	73%
149	Barium Molybdenum *Sulfate*	3000	680	100%	80%	90%	93%	67%

Notes:
NA - The CPC provides some protection from winds. Convection losses are ignored since they are assumed to be small relative to radiation losses.
* Average flux at entrance to CPC. Exit CPC flux is 5.6 times this value.
** Based on exit area of CPC.

Table 6. Receiver Efficiencies for Solar Dishes (Annual)

PID	Cycle Name	Aperture Flux kW/m^2	Thermal Losses kW/m^2	Absorb η	Radiation η	Convect η	Trans-ient η	Receiver Thermal η
00	Lo-T *Electrolysis* **BASELINE**	2500	127	100%	96%	97%	93%	86%
106	Hi-T Steam *Electrolysis*	2500	166	100%	94%	97%	93%	84%
2	Nickel-Iron Manganese *Ferrite*	4000	969	100%	68%	99%	93%	62%
7	Iron Oxide *Ferrite*	7000	1649	100%	69%	99%	93%	62%
194	Zinc *Ferrite*	4000	969	100%	68%	99%	93%	62%

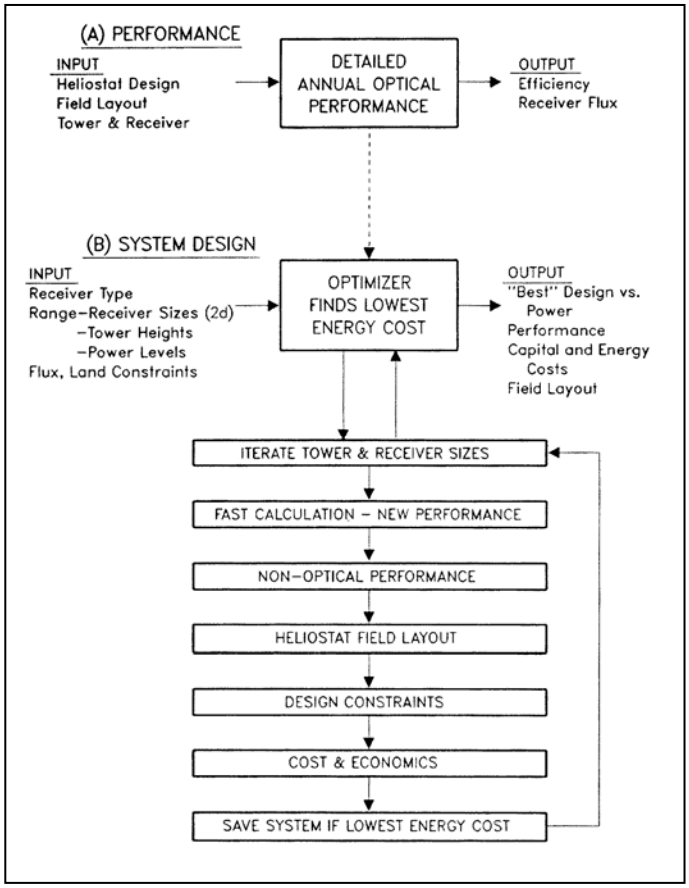

Figure 4. DELSOL Solar Tower Optimization Tool

- The optical efficiencies of the molten-salt plant (PID 191) and low-temperature particle plant (PID 67) are the same. From Table 3 we see that the particle plant has a higher cosine efficiency but lower efficiencies for atmospheric attenuation and aperture intercept. North heliostat fields have a higher cosine efficiency than surround heliostat fields. However, when all heliostats are to the north of the tower the heliostat beams must travel longer distances. This leads to higher atmospheric attenuation losses and larger beam sizes. The latter increases intercept losses. North fields also lead to taller towers to keep shading and blocking losses of the more distant heliostats to a minimum.

- The receiver efficiency for the particle receiver plant is somewhat lower (76% for PID 67) than the molten-salt plant (83% for PID 191). From Table 5 we see that one advantage of the cavity receiver is that it absorbs more of the incident light (~100% vs. 93%); the incident light experiences multiple reflections inside the cavity but only a single reflection on an external receiver. The particle receiver and salt receiver should have similar startup and cloud transient losses. Thus, both are predicted to have a transient efficiency of 93%. However, the higher temperature of the particle receiver leads to higher radiation and convection losses.

Interfacing the solid-particle-receiver plant with the sulfur hybrid plant (PID 67) or the cadmium sulfate plant (PID 147) is predicted to yield a 22% annual solar-to-hydrogen efficiency. Other combinations of the solid-particle plant and thermochemical cycles lead to lower efficiencies.

CPC/SiC Reactor Plant Calculations

The molten-salt and solid-particle plants described above were sized to absorb 700 MW_t within a single receiver on a single tower. Large plants like this usually enjoy economies of scale over small plants. Given this rationale, it would be desirable to scale up the CPC plant to as large a size as possible. However, use of the CPC concentrators reduces the number of heliostats that can be aimed at a single tower (see Figure 5). CU/NREL suggests that ~140 MWt may be the optimal size for a single receiver/tower [11]. Thus, five towers would be required to absorb 700 MW_t.

In the DELSOL analysis we studied the performance of only the north-facing CPC within the 140 MWt receiver, the most efficient of the three CPCs. This CPC absorbs ~1/3 of the total power, or 46 MW.

This calculation was based on the following DELSOL input:

- Heliostats – 98 m^2; 1.3 mrad slope/tracking error; 94% reflectance; 95% cleanliness; canted/focused to slant range; cost is \$120/m^2; heliostats are north of the tower within a +/- 24 degree sector of land.
- Receiver – CPC at receiver entrance with an acceptance angle of +/- 24 degrees, a geometric concentration of 6.2, and a throughput of 89%; receiver absorbs 46 MWt @ noon; 1550 ^oC to 1800 ^oC outlet temperature equates to thermal losses of 620 to 1010 kW per m^2 of CPC exit area; default cost algorithms for receiver and tower.

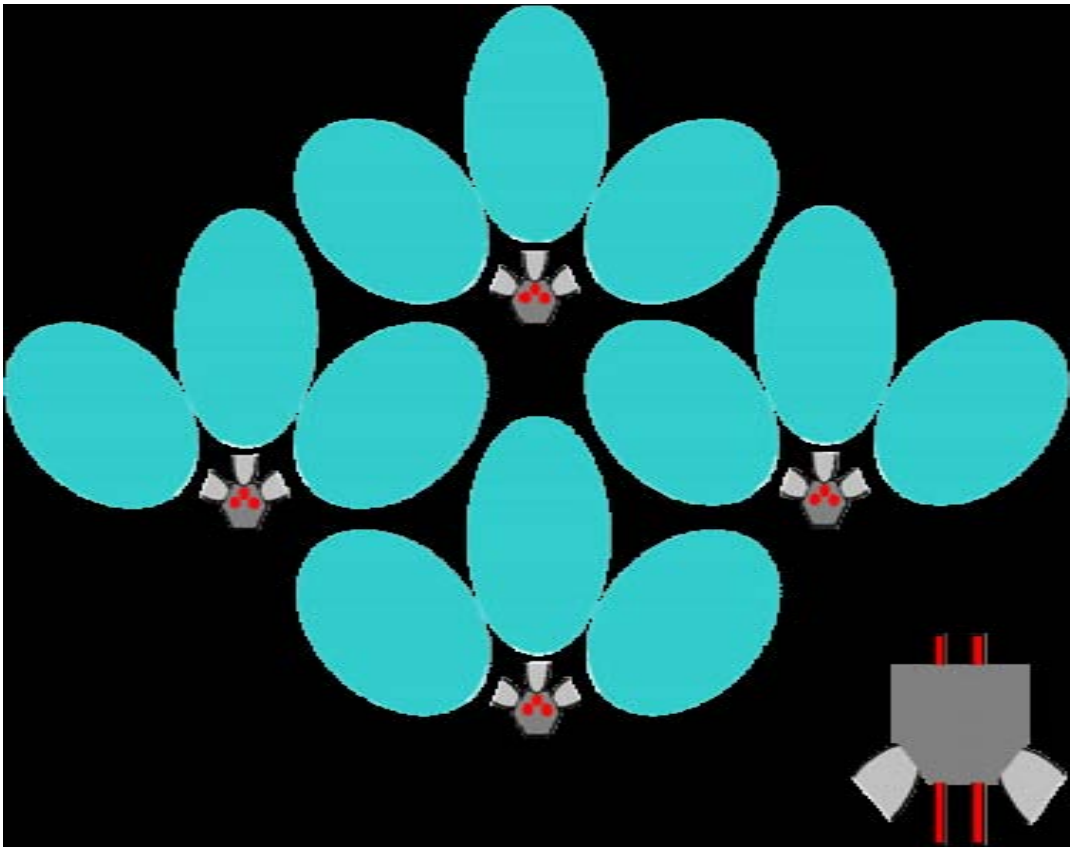

Figure 5. Compound parabolic concentrators.
The use of CPCs reduces the number of heliostat per tower, relative to a non-CPC tower, because the CPC only views a portion of the ground below the tower (blue ovals). Thus, multiple towers are typically required to build large plants.

The optimal field for the 1550 ^{o}C case is predicted to use 88,400 m^2 of heliostats, a 160-m tower, and a CPC tilted downward at 30^{o} with an entrance diameter of 9.5 m and an exit diameter of 3.8 m. Comparing these results with the solid-particle plant yields the following insights:

- The optical efficiency of the CPC plant is lower than the solid-particle plant. The main reason for this can be seen in Table 3; the CPC causes additional losses that do not apply to the solid particle plant. These losses are partially compensated by a higher atmospheric attenuation efficiency for the CPC plant; since the heliostat field is smaller, reflected beam distances are shorter, resulting in less attenuation.

- The receiver efficiencies of the CPC plant (PID 110) and low-temperature particle plant (PID 67) are approximately the same even though the CPC plant operates at much higher temperature (1600 ^{o}C vs. 900 ^{o}C). The 6.2 geometric concentration of the CPC greatly reduces heat loss through the aperture.

Interfacing the CPC plant with the manganese metal oxide cycle (PID 110) yields an annual solar-to-hydrogen efficiency of 23%. Interfacing with the higher temperature zinc cycle (PID 6) results in an efficiency of 16.5%.

Dish Plant Calculations

Like the power tower hydrogen efficiency calculations, the thermochemical design point efficiency was assumed to be equal to its annual efficiency. Because of the direct heating of the ferrite material and improved recuperation and reactivity expected at low turn down, we believe that this is a reasonable assumption, at least at this point.

To calculate dish annual efficiency, an Excel spreadsheet computer program utilizing typical meteorological year (TMY2) data for Dagget, California, Las Vegas, Nevada, and Albuquerque, New Mexico, were used. TMY2 data includes direct normal insolation, wind speed, ambient temperature, and other meteorological data compiled on an hour-by-hour basis for a number of locations throughout the United States [12]. Using this data the receiver efficiency was calculated on an hour-by-hour basis, and from these results we calculated the radiation and convection losses and efficiencies and the net amount of energy delivered to the thermochemical process over the year.

Calculation of dish optical efficiency is relatively straightforward compared to power towers. Identical reflectance (94%), dirt factors (95%), and field availability (99%) were used. Annual shading and blockage efficiency is 98% for a field of dishes. Because dishes continuously point at the sun, there are no cosine losses. Also, the short focal lengths result in no atmospheric attenuation losses. Aperture intercept for the baseline Stirling PCU/Electrolyzer and High Temperature Electrolysis is 99%. For the mixed-metal Ferrite cycles at 1800 ^{o}C, the intercept is reduced to 95% in order to achieve a higher average concentration ratio of 4000 suns. These concentration ratios are consistent with the 1.3 mrad slope error assumed for heliostat slope and tracking errors as well as the optical performance measured for the 10 kWe Advanced Dish Development System dish/Stirling concentrator [13]. Because the receiver window on the rotating disk reactor can be relatively large compared to the aperture and is located outside the cavity, it can operate at much lower temperatures than windows on power tower CPC receivers. Antireflective coatings and higher transmittance (95% vs. 90%) are, therefore, feasible on a dish receiver window. For Iron Oxide ferrite operating at 2100 ^{o}C, a trumpet concentrator is used to increase concentration ratio to 7000 suns. Trumpet concentrators (for the 2100 ^{o}C cycle) also utilize significantly fewer reflections than a CPC, resulting in a higher efficiency (96% vs. 89%), but at the expense of lower concentration (1.75 thermal vs. 6.2 geometric).

Receiver efficiency was calculated with TMY2 data by summing available direct normal insolation, losses, and delivered thermal energy over a typical meteorological year. Losses generally include radiation, convection, reflection, and conduction. Reflection losses are typically less than 1 percent for cavity receivers. An absorption efficiency of 100% was, therefore, assumed. Conduction losses are also typically negligible. Convection losses for the open cavity Stirling PCU receiver is an estimate based on mixed forced and natural convection for a cavity solar receiver at a 40-degree elevation angle. Convection losses for the windowed rotating disk reactor accounts for convection from the window. Radiation losses are by far the

largest heat loss mechanism. The Stefan-Boltzmann radiation law assuming that the receiver cavity aperture radiates at the high temperature with an emissivity of 0.99 for the Stirling PCU and 0.90 for the rotating disk reactor windowed receiver was used to calculate annual radiation efficiency. The transient efficiency, 93%, accounts for the approximately 4% of the direct normal insolation at levels below the operational threshold of 300 W/m^2 and a 0.97 empirical factor for thermal transient losses.

It is important to note that the very high operating temperature of 1800 ^oC for the mixed-metal Ferrite cycles results in a low annual receiver efficiency of only 62%. If the receiver temperature could be reduced to 1500 ^oC, as recent experimental results suggest they might, receiver efficiency increases to 76% — a 22% increase. Given the uncertainty in the receiver temperature requirements and the sensitivity of annual system efficiency to receiver temperature, especially for the very high temperature cycles, it is important not to place too much faith on the precision of these results.

CONCLUSIONS

The screening analysis identified a number of concepts that potentially could produce hydrogen at efficiencies significantly higher than low-temperature electrolysis.

Some general qualitative conclusions can also be drawn:

- No parabolic trough concepts were identified.

- Although CSP systems are capable of operating at very high temperatures, to maximize annual efficiency operating temperatures are limited by radiation losses. The following are general temperature limits for tower and dish receiver concepts:
  - Surround tower, molten salt ~600 ^oC
  - North facing tower, solid particle ~1200 ^oC
  - North facing high performance tower, CPC ~1600 ^oC
  - Parabolic dish, rotating disk reactor ~1800 ^oC

- The solar collection efficiency (i.e., product of optical and receiver efficiencies) of the CPC plant exceeds the solid particle plant above ~1400 ^oC.

- The efficiency of high-temperature steam electrolysis concepts are similar to the best thermochemical concepts.

- For the very high temperature cycles (>1500 ^oC), radiation losses dominate and receiver efficiency is extremely sensitive to temperature.

The numerical results presented here are "1st-order estimates" and should be updated as new information becomes available.

REFERENCES

1. P.I. Pohl, L.C. Brown, Y. Chen, R.B. Diver, G.E. Besenbruch, B.L. Earl, S.A. Jones, and R.F. Perret, Evaluation of Solar Thermo-Chemical Reactions for Hydrogen Production, *Proceedings of the 12th International Symposium Solar Power and Chemical Energy Systems*, Oaxaca, Mexico, October 2004.

2. University of Nevada (Las Vegas), Solar Hydrogen Generation Research, Project Progress Reports through 2007, http://shgr.unlv.edu/v2/.

3. Boeing Aerospace Company, *Small Central Receiver Brayton Cycle Study Final Technical Report*, SAND84-8189. Sandia National Laboratories, Livermore, CA, 1985.

4. A.F. Hildebrandt, and K.A. Ross, Receiver Design Considerations for Solar Central Receiver Hydrogen Production, *Solar Energy*, Vol. 35, No. 2, pp. 199-206, 1985.

5. A. Steinfeld and R. Palumbo, "Solar Thermochemical Process Technology," *Encyclopedia of Physical Science and Technology*, R. A. Meyers, Ed., Academic Press, Vol. 15, pp. 237-256, 2001.

6. J.M. Hruby, *A Technical Feasibility Study of a Solid Particle Solar Central Receiver for High Temperature Applications*, SAND86-8211. Sandia National Laboratories, Albuquerque, NM, March 1986.

7. Babcock & Wilcox, *Selection and Conceptual Design of an Advanced Thermal Energy Storage Subsystem for a Commercial Scale (100 MWe) Solar Central Receiver Power Plant*, SAND80-8190. BAW-1662, February 1981.

8. Computer program, "Outokumpu HSC Chemistry for Windows," Version 5.1 (HSC 5), Antti Roine, 02103-ORC-T, Pori, Finland, 2002.

9. B.L. Kistler, *A User's Manual for DELSOL3: A Computer Code for Calculating the Optical Performance and Optimal System Design for Solar Thermal Central Receiver Plants*, SAND86-8018. Sandia National Laboratories, Albuquerque, NM, November 1986.

10. Sargent & Lundy, *Assessment of Parabolic Trough and Power Tower Solar Technology Cost and Performance Forecasts*, SL-5641, May 2003.

11. A. Weimer, A. Lewandowski, C. Perkins, and J. Zartman, "ZnO/Zn Preliminary Economics," input to H2A year 2025 case study, University of Colorado, January 17, 2006.
12. W. Marion and K. Urban, *User's Manual for TMY2s Typical Meteorological Years*, National Renewable Energy Laboratory, Golden, CO, 1995.

13. R.B. Diver, C.E. Andraka, K.S. Rawlinson, V. Goldberg, and G. Thomas, The Advanced Dish Development System Project, *ASME Proceedings of Solar Forum 2001*, Washington, D.C., 2001.

DISTRIBUTION

1 U.S. Department of Energy
Attn: R. Farmer
Hydrogen and Fuel Cell Program
1000 Independence Avenue, SW
Washington, DC 20585

1 Robocasting Enterprises
Attn: J.N. Stuecker
4501 Bogan #B4
Albuquerque, NM 87109

3 General Atomics
Attn: L.C. Brown
G. Besenbruch
B. Wong
P.O. Box 85608
San Diego, CA 92186

1 Los Alamos Renewable Energy
Attn: Reed Jensen
19 Industrial Park Rd
Pojoaque, NM 87506

1 Dave Patterson
1240 Gilbert Ave
Downs Grove, IL 60515

1 Edward A. Fletcher
3909 Beard Ave. S.
Minneapolis, MN 55410

1 R.F.D. Perret
3004 Hawksdale Drive
Las Vegas, NV 89134

1 TIAX LLC
Attn: K.W. Roth
15 Acorn Park
Cambridge, MA 02140

1 Niigata University.
Attn: Dr. Tatsuya Kodama
Department of Chemistry & Chemical Engineering
8050 Ikarashi 2-nocho, Niigata 950-2181
Japan

2 Texas Tech University
Attn: D.L. James
Department of Mechanical Engineering
Box 41021
Lubbock, TX 79409

2 DLR
Attn: Christian Sattler
Martin Roeb
Linder Hoche
51147 Cologne
Germany

1 ETH Zurich
Attn: Aldo Steinfeld
ETH Zentrum ML-J42.1
8092 Zurich
Switzerland

1 University of Colorado
Attn: Al Weimer
Chemical Engineering Department
Boulder, CO 80309-0424

4 University of Nevada, Las Vegas
Attn: Sean Hsieh
Taide Tan
Yitung Chen
Roger Rennels
4505 Maryland Parkway, Box 4027
Las Vegas, NV 89052

1 Gilles Rodriguez
CEA-Centre de Cadarache Bât.208
DEN/DTN/STPA/LPC
13108 St Paul lez Durance – France

1	Pietro Tarquini ENEA – TER – Solterm-Svil - C.R. Casaccia Via Anguillarese,301 - 00060 Santa Maria di Galeria Roma - Italia	
2	MS0836	R.E. Hogan, 1516
1	MS1110	J.S. Nelson, 6337
8	MS1127	R.B. Diver, 6337
2	MS1127	NSTTF Technical Library, 6337
1	MS1127	T.A. Moss, 6337
1	MS1127	N.P. Siegel, 6337
8	MS1127	G.J. Kolb, 6335
1	MS1349	C. Apblett, 1815
1	MS1349	E. Branson, 1815
1	MS1349	L. Evans, 1815
2	MS1349	J.E. Miller, 1815
1	MS9052	J.O. Keller, 8367
1	MS9054	D.R. Hardesty, 8360
1	MS9291	M.D. Allendorf, 8324
1	MS0899	Technical Library, 9536 (electronic copy)


Sandia National Laboratories